PHYSICAL REVIEW B VOLUME 8, NUMBER 6 15 SEPTEMBER 1973

Temperature Dependence of Second-Order Raman Scattering in Potassium and Rubidium Halides*

J. E. Potts and Charles T. Walker
Physics Department, Arizona State University, Tempe, Arizona 85281

Indira R. Nair†
Physics Department, Northwestern University, Evanston, Illinois 60201

(Received 13 September 1972)

The second-order Raman-scattering spectra of KCl, KBr, KI, RbCl, RbBr, and RbI have been recorded at 300, 90, and 23 K. A symmetry analysis for reducing phonon pairs into irreducible representations has been employed, in conjunction with a knowledge of the one-phonon densities of states derived from neutron-diffraction data, to identify the two-phonon combinations that give rise to features in these second-order Raman spectra. The temperature dependence of a given spectrum is dominated by the phonon occupation numbers which appear in the final-state density-of-states factor in the scattering cross section. In addition to a description of the general features of the second-order spectra, the results for each substance are described and discussed individually in some detail.

I. INTRODUCTION

The purpose of this paper is to report the measurements of the second-order Raman spectra for the alkali halides KCl, KBr, KI, RbCl, RbBr, and RbI at 300, 90, and 23 K. The Raman spectra of these halides, with the exception of RbBr, have been studied previously by different workers[1-6] and the results of most of this work have been summarized by Krishnan[7] and Krauzman.[1] All the earlier data, however, were taken at 300 K and some of the work was done using mercury-arc excitation, making the identification of the weak second-order bands difficult. Further, the dispersion curves of the rubidium halides were not available at the time.

First-order Raman scattering phonons is governed by a third-rank tensor $\alpha^{\mu}_{\rho\sigma} = \partial \alpha_{\rho\sigma}/\partial Q_{\mu}$, viz., the first derivative of the polarizability tensor $\alpha_{\rho\sigma}$ with respect to the phonon coordinate Q_{μ}.[8] In the alkali halide crystals, every atom is at a center of inversion symmetry and hence every element of a third-rank tensor property of a crystal should be identically zero for these crystals. Thus, first-order Raman scattering is forbidden in the pure alkali halides. Second-order spectra have been observed and calculated for different alkali halides by various workers.[9-11] Temperature dependence of second-order spectra is of intrinsic interest by itself, but, in addition, knowledge of the second-order spectra is important in separating the first- and second-order contributions to the Raman spectra induced in alkali halides by substitutional impurities, particularly when the first-order polarizability derivatives are still small so that the intensities of the host second-order spectrum and the impurity-induced first-order spectrum are comparable.[12,13] In these cases, the temperature dependence of the spectra is also necessary to distinguish first- from second-order scattering.[14]

II. SECOND-ORDER RAMAN SCATTERING BY PHONONS

A. Mechanism and General Features of the Spectrum

Second-order Raman scattering by phonons is a process in which the incident light is inelastically scattered by the phonon system of the crystal, resulting in a change of the phonon occupation number by two. Loudon[15] has indicated the possible mechanisms for second-order Raman scattering in an "harmonic" crystal, viz., two successive first-order processes or a single four-vertex process in which the two phonons are generated essentially because of the electron-phonon interaction. Of these only the second process is allowed in an alkali halide because of inversion symmetry. This process corresponds to a second-order polarizability mechanism involving the second-order derivatives of the polarizability with respect to the phonon coordinates. Another possible mechanism is via an anharmonic interaction, but again this mechanism can contribute to second-order scattering only when first-order scattering is allowed and hence is ruled out in the case of alkali halides.

Conservation of momentum in a periodic crystal demands that the sum of the wave vectors of the two phonons participating in the second-order Raman scattering process balance the change in wave vector between the incident and scattered photons. As the photon wave vectors are essentially zero ($\sim 10^{-3}$) compared to the extent of the Brillouin zone, the wave vectors of the phonons involved should be (very nearly) equal and opposite. Thus, the phonons that would combine would be those on the same or different branches of the

dispersion curve at the same point of the Brillouin zone.

The symmetry analysis and selection rules for reducing phonon pairs into irreducible representations and obtaining the combinations that give rise to second-order Raman scattering and infrared absorption have been worked out by Birman[16] and by Burstein, Johnson, and Loudon.[17] All combinations at the Γ and X points are forbidden in infrared two-phonon absorption in alkali halides, while most combinations are allowed in Raman scattering. This gives rise to a considerable amount of structure in the second-order Raman scattering spectra as compared to the two-phonon infrared absorption spectra. As the Raman selection rules are not severly restrictive, the frequency dependence of the Raman spectrum reflects the two-phonon density of states. Thus, one can expect an examination of the critical points in the one-phonon density of states to reveal the positions of the features in the two-phonon Raman spectrum. The indexing of the second-order features as being due to combinations at the critical points, called the critical-point analysis, has been commonly used in describing the second-order Raman spectra.

A second-order process can be one in which both phonons are created, both destroyed, or one created and one destroyed. The Raman shift is on the Stokes side in the first case, the anti-Stokes side in the second case, and can be on the Stokes or anti-Stokes side in the third case, depending upon whether the frequency of the phonon created is greater than or less than that of the phonon destroyed. The corresponding frequency shifts are $\pm\omega_1 \pm \omega_2$, where ω_1 and ω_2 are the frequencies of the participating phonons. Because of the pos-

TABLE I. Symmetry reduction of Raman-active two-phonon combinations at different points in the Brillouin zone.

Point or direction	Phonon branches polarizations	Combinations	Reduced Raman-active combinations
Γ	LO	2LO	$A+E+T$
	TO	2TO	$A+E+T$
	$\omega(A)=0$	LO ± TO	$A+E+T$
Δ	LA, LO	2LA, 2LO	$A+E$
and X	TA, TO	2TA, 2TO	$A+E+T$
		LA ± LO	$A+E$
		LA ± TA, LO ± TA, LA ± TO, LO ± TO	T
		TA ± TO	$A+E+T$
Λ	LA; LO	2LA, 2LO	$A+T$
	TA; TO	2TA, 2TO	$A+E+2T$
		LA ± LO	$A+T$
		LA ± TA, LO ± TA, LA ± TO, LO ± TO	$E+T$
		TA ± TO	$A+E+2T$
L	LA; LO	2LA, 2LO	$A+T$
	TA; TO	2TA, 2TO	$A+E+T$
		LA ± LO, LA ± TO, TA ± LO, TA ± TO	not allowed
		LA ± TA, LO ± TO	$E+T$
W	W_1^T, W_2^T	$2W_3$, $W_3 \pm W_3$	$A+2E+T$
	$2W_3$	$2W_1$, $2W_2$	$A+E$
		$W_1 \pm W_2$	E
		$W_1 \pm W_3$, $W_2 \pm W_3$	T
Σ	LA, LO	2LO, 2LA, 2TO{xy}, 2TA{xy}, 2TA{z}, 2TO{z}	$A+E+T$
	TA{z}, TO{z}	TA{z} ± TA{xy}, TA{z} ± TO{xy}, TO{z} ± TA{xy}, TO{z} ± TO{xy}	T
	TA{xy}, TO{xy}	TA{xy} ± LA, TA{xy} ± LO, TO{xy} ± LO, TO{xy} ± LA	E
		TA{z} ± LA, TA{z} ± LO, TO{z} ± LA, TO{z} ± LO	T
		TA{z} ± TO{z}, TA{xy} × TO{xy}, LA ± LO	$A+E+T$

sibility of scattering all over the Brillouin zone, the second-order Raman spectrum is a quasi-continuous spectrum starting at essentially zero frequency with the difference bands $(\omega_1-\omega_2)$ concentrated mainly in the lower-frequency regions and the summation bands $(\omega_1+\omega_2)$ in the higher-frequency regions. Only the Stokes spectra have been studied in the present work as the anti-Stokes spectrum does not yield any additional information about phonon frequencies and is of much weaker intensity. As third-order scattering is forbidden in alkali halides, and since the highest phonon frequency occurs for the LO phonon at the point Γ, the second-order spectrum must have a cutoff at twice the frequency of the LO(Γ) phonon.

B. Selection Rules for the Alkali Halides

As mentioned earlier, Birman[16] and Burstein *et al.*[17] have obtained the allowed phonon combinations contributing to the second-order spectra of the alkali halides. Burstein *et al.*[17] have tabulated the particular combinations for each symmetry point. For the assignment of each band, however, it is useful to know the irreducible representation into which each allowed combination reduces (i.e., the Kronecker product of the representations of the combining phonons in the case of combinations like $\omega_1+\omega_2$ and the symmetrized square for the harmonics like $2\omega_1$.) This is indicated for the important symmetry points and directions in Table I.

The alkali halides considered in this paper all belong to the symmorphic space group O_h^5. The irreducible representations of the point group O_h (symmetry group of the point Γ) which are symmetric under inversion and, hence, can contribute to Raman scattering are A_{1g}, E_g, and T_{2g}.[15] In the experimental observations one can determine the elements of the scattering tensor which contribute to the scattered intensity in a particular geometry and accordingly classify the phonon combinations giving rise to the scattering as being reducible to one or more of the symmetries A_{1g}, E_g, or T_{2g}.

Combinations for the main symmetry lines and for the points of high symmetry are shown. In all alkali halides of fcc structure the transverse branches are degenerate along the directions $\Delta[100]$ and $\Lambda[111]$, giving rise to four branches in this region of the Brillouin zone. Along the $\Sigma[110]$ direction and along XW (usually denoted by Z) the degeneracy is lifted and there are six distinct phonon branches, merging to four points again at W. This explains the various possible combinations considered in Table I. The superscripts on the branches indicate the polarization of the phonon in the cases where it can be defined.

The most complete experimental work on second-order spectra of KCl, KBr, and KI has been that of Krauzman who selected orientations of the crystal and polarizations of the incident and scattered light so that it was possible to observe combinations of symmetries A_{1g} and E_g simultaneously, E_g alone, or T_{2g} alone. It is not possible to observe A_{1g} symmetry alone because it has a diagonal representation in all the coordinate systems of the crystal and cannot be separated from the elements of the scattering tensor for E_g symmetry by any choices of coordinate system. In this work, we have used the goemetries of Krauzman to observe the combinations. The frequencies of the various second-order features are then compared with possible phonon combination frequencies obtained from the neutron data.

In the critical point analysis, it is customary to consider the zone-boundary points Γ, L, X and the symmetry point W primarily because zone-symmetry points are all critical to a greater or smaller extent.[18] However, in the case of alkali halides, the zone-boundary points above do not account for all the strongest features of the density of states. For instance, the strongest peak in the one-phonon density of states of KCl arises from a saddle point in the highest branch. Further, all alkali halides have a singularity in their density of states related to a near degeneracy of a saddle point near (0.5, 0.5, 0) and a maximum near L, as pointed out by Copley *et al.*[19] Similar features have to be taken into account when assigning two-phonon combinations to second-order features.

C. Temperature Dependence

The principle temperature dependence of the Raman spectra arises from the dependence of the scattering cross section on the phonon occupation number. A Stokes process giving rise to a frequency shift of ω_1 has a temperature dependence $n(\omega_1, T)+1$, where $n(\omega, T)$ is the Bose-Einstein factor $(e^{\hbar\omega/kT}-1)^{-1}$ for a phonon of frequency ω when the crystal temperature is T, while an anti-Stokes process of shift ω_1 has a dependence $n(\omega_1, T)$. Combinations of these processes give rise to the second-order spectra and the temperature dependences of the various possible combinations are shown in Table II.

Because of the Bose-Einstein factor the spectra become weaker at lower temperatures. However, the temperature factor for the intensity of summation bands $(\omega_1+\omega_2)$ is proportional to the product of two Stokes factors and is therefore greater than the corresponding difference band by $n(\omega_2, T)+1$. As temperature falls, the intensity drop in the summation-band region is not as great as in the difference-band region. Thus, the spectra at different temperatures often have a different appearance, the higher-frequency region (summation band) appearing enhanced at the lower tempera-

TABLE II. Temperature dependences of two-phonon combinations.

Frequency shift		Temperature dependence	Frequency region
Summation band	$\omega_1+\omega_2$	$[n(\omega_1, T)+1]\,[n(\omega_2, T)+1]$	Stokes (S)
	$-(\omega_1+\omega_2)$	$[n(\omega_1, T)]\,[n(\omega_2, T)]$	Anti-stokes (A)
Differences band $\omega_2+\omega_1$		$[n(\omega_2, T)+1]\,[n(\omega_1, T)]$	S or A depending on whether $\omega_2>\omega_1$ or $\omega_2<\omega_1$

tures. In the case of the spectra where the higher intensity is concentrated at the lower-frequency region arising mainly from difference bands at 300 K, the intensity is often reversed at lower temperatures, with the higher intensity in the high-frequency region.

The anharmonic interactions in the crystal are manifested in the temperature dependence of the spectrum primarily in two ways. The bands narrow as temperature decreases and shift in frequency, reflecting the change in phonon lifetime and frequency. Though phonons at different points undergo different frequency shifts, the shifts are usually of the same order of magnitude (~ 10–20 cm^{-1} from 300 to 80 K). This results in the fact that though difference bands narrow as temperature falls, they remain essentially constant in frequency while in the case of summation bands the shifts of the participatory phonons add to give rise to approximately twice the shift of a single phonon. The "true" width of each combination band must be approximately the sum of the widths of the phonons. However, the width of the observed bands are much higher because each band is a superposition of many phonon combinations.

Cowley[11] has calculated the second-order spectra for NaI and KBr using the shell model with anharmonic interactions between the ionic dipole moments. He has calculated the KBr spectra for various temperatures and different polarizations of the incident and scattered light. The shift of the Raman bands arising from phonon shifts are not exhibited by the calculated spectra because only the quasiharmonic frequencies at 90 K obtained from neutron measurements were used in the calculations. The only temperature dependence of these calculated spectra is in the intensity which falls with temperature.

Another effect on the frequencies of phonon combinations can also be expected from anharmonicity. The phonon-phonon interaction has the consequence that the energy of a phonon is modified by the presence of a second, and hence the energy of excitation of a pair or a group of phonons does not equal the sum of their excitation energies. Thus in the presence of anharmonicity, the observed second-order peak frequency might be expected to be different from the combination frequency calculated from the data from a one-phonon scattering experiment such as neutron scattering. In the case of alkali halides the observed frequency would usually be expected to be lower than calculated because available neutron data for alkali halides show anharmonicity to reduce most of the phonon frequencies.

We have included in Appendix A a critical point analysis for the six alkali halides studied here. The present work is concerned with the temperature dependence of second-order Raman spectra, and in order to analyze the data to see if the predominant temperature effect is that expected from simple phonon occupation number considerations, one must have knowledge of which phonon combinations correspond to the various features. The most straightforward way to obtain this information is to use a critical point analysis for assignment of the features. Critical point analyses have not been published for all six of the alkali halides studies here, and only two of the published analyses (KBr and KI) are directly based on phonon spectra obtained from inelastic neutron scattering. With neutron data now available for all six materials studied here, it is possible to rectify omissions in the published analyses,[1] particularly with respect to including interior critical points.

It would obviously be desirable to compare our data directly with calculations of the sort reported in Ref. 11. For the materials of interest to us such calculations have only been done for KBr. Further, these calculations depend to some extent on the preexistence of the data in order to fix some of the parameters in the calculation. It would seem instead that with the existence of a systematic collection of data at low temperatures one can now proceed to calculations using phonons appropriate to low temperatures, and avoid the difficulties introduced by the necessary consideration of anharmonic effects[11] in room-temperature calculations.

III. EXPERIMENTAL PROCEDURES

The crystals were grown by the Kyropoulos method from pure alkali halides obtained from Merck. The salts were dried and the chlorides were chlorine treated to remove OH^- impurities before the crystals were grown.

The exciting source in these experiments was a Spectra Physics 165 argon-ion laser giving 1.8 W in the 5145 Å line. Light scattered at 90° to the incident beam was passed through a rotatable polarizing sheet and a polarization scrambler and then dispersed by a Spex 1402 Double Monochromator. Signals were detected using a thermoelectrically cooled ITT-*FW*-130 photomultiplier tube in conjunction with an SSR-1120 amplifier and 1105 data converter console. A spectral slit width of 0.7 Å(~ 3 cm^{-1}) was used. Typical scan speeds

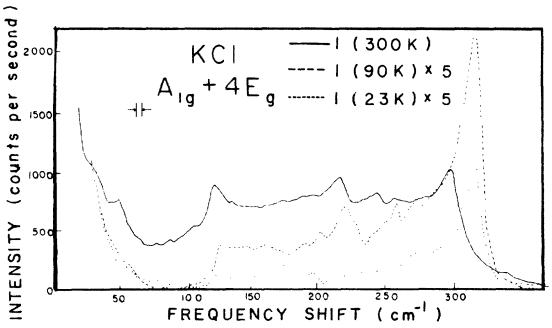

FIG. 1. Temperature dependence of the second-order Raman spectrum of KCl; $A_{1g}+4E_g$ symmetry.

were 1 Å/min with a detector time constant of 10 sec or 2 Å/min with a 5-sec time constant. These slow scans are necessitated by the weak intensity of the second-order scattering.

The spectrometer drive was found to be less than perfectly linear in wavelength. However, the frequency shifts are marked every 50 cm^{-1} in the spectra reported here to enable an accurate interpolation of peak positions.

The geometries used were $z(yy)x$, $z(yz)x$, and $z(x'y')x'$, where $x=[100]$, $y=[010]$, $z=[001]$, $y'=[1\bar{1}0]$, and $x'=[110]$ (using the notation of Ref. 20). The corresponding spectra reflect intensities corresponding to the different symmetries $I(A_{1g})+4I(E_g)$, $I(T_{2g})$, and $3I(E_g)$, respectively.

An optical cryostat of conventional design was used with liquid nitrogen and liquid helium for low-temperature measurements. The fixed temperatures thus obtained were 90 ± 2 and 23 ± 2 K, which were constant to 1 K during each run, as measured by a 1000-Ω, $\frac{1}{8}$-W, Allen Bradley resistor thermally bonded to the copper sample holder.

IV. RESULTS

The Raman spectra for the alkali halides studied are shown in Figs. 1–18. It is observed that these spectra, though continuous as expected from the possibility of scattering throughout the Brillouin zone, have certain predominant features, such as peaks and shoulders. The positions of these features at the different temperatures and the frequencies of the comparable two-phonon combinations at critical points obtained from the neutron data are shown in Tables IX–XIII. The salient features of the temperature dependence of the spectra for each of the crystals studies are discussed separately below. In each case, the spectra for each sample are recorded in three figures. Each figure shows the spectra for a single polarization for the three temperatures 300, 90, and 23 K. Spectral slit widths are indicated by the vertical bars. The first figure in each case contains the intensity $I(A_{1g})+4I(E_g)$, the second $I(E_g)$, and the third $I(T_{2g})$. The intensity scale is in units of counts per second. Because of the different geometries and sizes of crystals involved an accurate intensity comparison cannot be made from crystal to crystal, but an estimate of the relative intensity of one crystal with respect to another may be obtained. The ratio of the scattering by components of different symmetry, i.e., $I(A_{1g}):I(E_g):I(T_{2g})$ may be obtained by measuring the total area under the spectra. The strongest bands of each symmetry are indicated by asterisks in the Tables IX–XIII.

A. KCl

Figures 1–3 show the Raman spectra for KCl; Table IX shows the frequencies of prominent features and their assignments. The most intense part of the spectrum is the scattering due to the A_{1g} component of the combinations. By measuring the area under the spectrum from the initial "dip" at the foot of the exciting line to the apparent cutoff, the ratio $I(A_{1g}):I(T_{2g}):I(E_g)$ is obtained as $\simeq 60:6:1$ at 300 K. This is only an approximate value because the "dip" has to be judged arbitrarily. The figures also show the temperature dependence of the scattering. The intensities for the spectra at 90 and 23 K have been multiplied by five in order to show the features of the low-temperature spectra clearly. The general features of the dependence are at once obvious. The decrease of in-

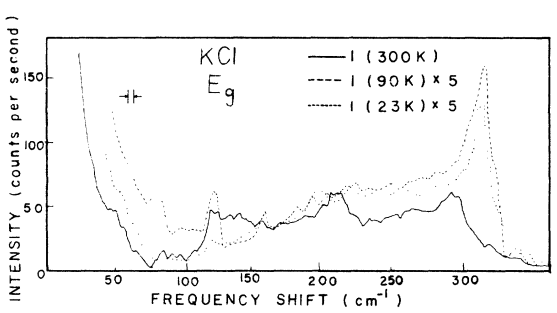

FIG. 2. Temperature dependence of the second-order Raman spectrum of KCl; E_g symmetry.

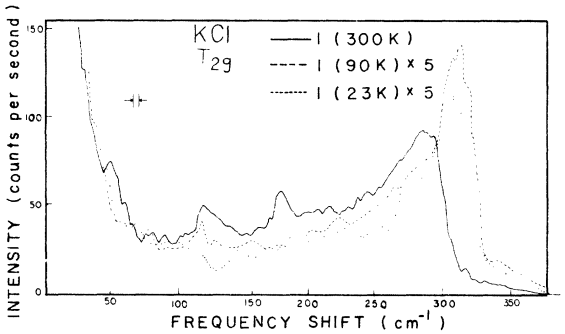

FIG. 3. Temperature dependence of the second-order Raman spectrum of KCl; T_{2g} symmetry.

TABLE III. Temperature dependence of some features of KCl second-order Raman spectrum.

Raman shift (cm^{-1}) (300 K)	Combinations contributing to the band	Intensity ratio $I(300):I(90):I(23)$ Calculated	Observed
50	LA − TA(X)	280: 28: 1	10: 1: 1
	LO − LA(X)	2500: 200: 1	uncertain
118	2TA(X)	16: 2.5: 1	15: 2: 1 (combined)
166	LA + TA(X)	10: 2: 1	8: 1: 1
290	2TO(X)	3.6: 1.2: 1	3.6: 1.2: 1 (combined)
	LO + TO(X)	3.3: 1.1: 1	

tensity with temperature is much higher for the difference bands than the summation bands, so that the summation bands appear enhanced at lower temperatures. The intensity ratios may be calculated assuming a temperature dependence due to phonon occupation numbers alone as explained in Sec. II. For a correct intensity comparison, the areas under the peaks due to scattering from a given combination should be measured and compared. This is impossible in the present situation because each band is actually a superposition of bands arising from the scattering due to different combinations of the same combination frequency, but each having a different temperature ratio. Because of this only the heights of peaks can be compared, assuming that each peak arises from a single combination. Even under this assumption, comparison of intensities poses a problem because most combinations reduce to more than one irreducible representation and the intensity ratio in these cases should be taken by combining the intensities contributed by each combination to the different irreducible components. In Table III, which gives the ratios of intensities at the three temperatures for a few of the bands, those ratios denoted by "combined" were determined in this manner.

The calculated ratios show the contrast between difference and summation bands immediately. The calculation of the difference bands ratio from the spectra proved difficult because the peaks ride on the Rayleigh line. For the other bands the observed and calculated intensities compare well. In particular, for the band of the highest frequency the various assignments give calculated intensity ratios close to each other because they are all combination bands arising from phonons of frequencies very close to each other. In this case comparison with the observed value is exceptionally good.

The shifting and broadening of the frequencies with temperature are also observed. The difference band region is essentially constant while the summation region shifts by almost 15–20 cm^{-1} from 300 to 90 K but very little from 90 to 23 K. The lines also narrow as temperature falls but not by a large amount because the main source of the peak width is the superposition of different combinations rather than the anharmonic effects.

B. KBr

Figures 4–6 show the spectra for KBr and the assignments are discussed in Appendix A. The most intense component is again the A_{1g} spectrum. The ratio $I(A_{1g}):I(E_g):I(T_{2g})$ is 24: 1.1: 1 so that the E_g and T_{2g} components in this case are almost equal in intensity.

Table IV shows the ratios of intensities at 300, 90, and 23 K for the main features. The agreement between calculated and experimental values

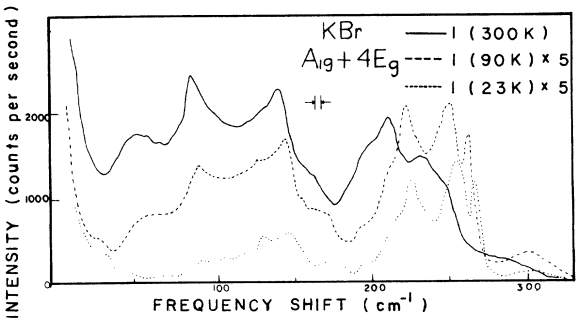

FIG. 4. Temperature dependence of the second-order Raman spectrum of Kbr; $A_{1g}+4E_g$ symmetry.

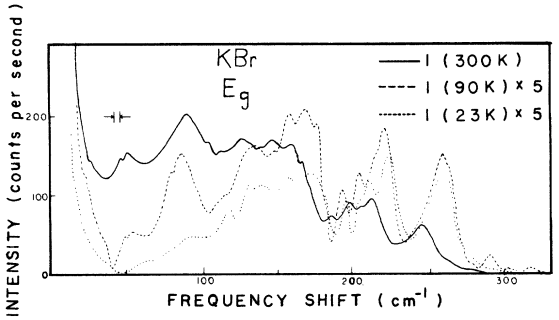

FIG. 5. Temperature dependence of the second-order Raman spectrum of KBr; E_g symmetry.

TABLE IV. Temperature dependence of some features of KBr second-order Raman spectrum.

Raman shift (cm^{-1}) (300 K)	Combinations contributing to the band	Intensity ratio $I(300): I(90): I(23)$ Calculated	Observed
50	$LO-LA(X)$	420: 44: 1	400: 36: 1
86	$2TA(X)$	26: 3.5: 1	28: 4: 1 (combined)
121	$TA+LA(X)$	17: 3: 1	15: 3: 1
142	$2LA(X)$	11: 2: 1	10.5: 2: (combined)
217	$2TO(X)$	5: 1.5: 1	3.5: 1.5: 1 (combined)

is extremely good. This is possibly because the higher intensity of the spectrum and the better definition of the peaks in this case enable a better estimate of the intensity ratios from the spectrum. The difference in the intensity ratios in the case of difference and summation bands is at once obvious. The high-frequency bands also resolve well into components at lower temperatures. The intensity ratio for the strong T_{2g} band agrees closely with the calculated value, indicating that it is almost completely due to a single combination scattering, and not a superposition of combinations.

Another interesting observation can be made concerning the observed shifts of the Raman peaks. The neutron data in Ref. 21 indicate that in going from 400 to 90 K, the TO modes show a constant increase in frequency of about 8%, the LO modes about 4%, the LA modes shift slightly but only for a few points along Δ and Σ, and the TA modes are unshifted. This trend is reflected in Table IV. The lower-frequency difference modes shift by about 6–8% when the combination involves one optical mode and one acoustic mode and does not shift at all when both modes are acoustic and at zone-boundary points as in the case of the $2TA(X)$ band at 86 cm^{-1} and the $TA+LA(X)$ band at 121 cm^{-1}. When the combination involves one LA mode at an interior zone point as in $LA+TA(\Sigma)$ (142 cm^{-1}) there is a slight shift observed. Again in the summation region, the $2TO(X)$ band is shifted by 15% whereas the $LO+LA(\Sigma)$ band only shifts 4%.

C. KI

Figures 7–9 show the Raman spectra for KI and the assignments of features are discussed in Appendix A. The total ratio $I(A_{1g}): I(E_g): I(T_{2g})$ is 40: 1: 3.

The temperature dependence is clear from the figures. In particular, the E_g spectrum of Fig. 8 shows the striking difference in the intensity ratio between the difference band at 65 cm^{-1} and the summation band at 100 cm^{-1}. Table V shows the comparison of the calculated and observed values. The agreement is poor for the difference band and is not as good as in the case of KBr for the other bands. This is possibly because the bands are due to superposition of many combinations and a true intensity comparison is not possible. The calculated ratio for the combination assigned to Σ' agrees surprisingly well with the observed value.

The bands shift 5–10% in going from 300 to 90 K. The neutron data at 300 K are not available for comparison. There is very little shift as the temperature is lowered from 90 to 23 K.

D. RbCl

Figures 10–12 show the Raman spectra for RbCl and the assignments are given in Appendix A. The intensity ratios at 300 K are 30: 2: 3 for the three polarizations $I(A_{1g}): I(E_g): I(T_{2g})$.

The temperature dependence is striking. Table VI shows that the observed intensity ratios agree fairly well with the experimental values. At

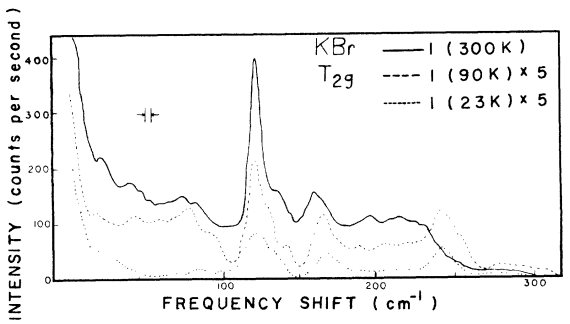

FIG. 6. Temperature dependence of the second-order Raman spectrum of KBr; T_{2g} symmetry.

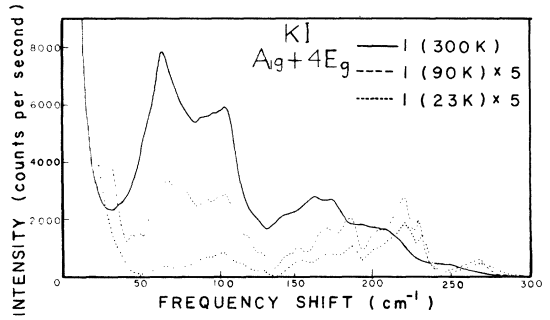

FIG. 7. Temperature dependence of the second-order Raman spectrum of KI; $A_{1g}+4E_g$ symmetry.

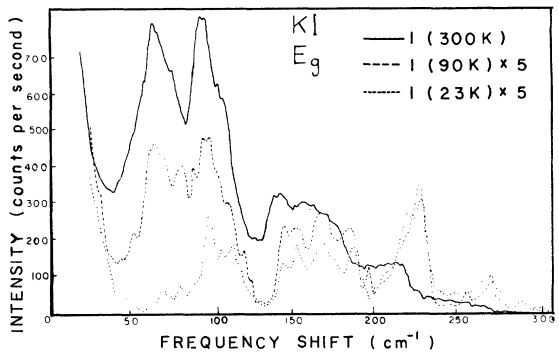

FIG. 8. Temperature dependence of the second-order Raman spectrum of KI; E_g symmetry.

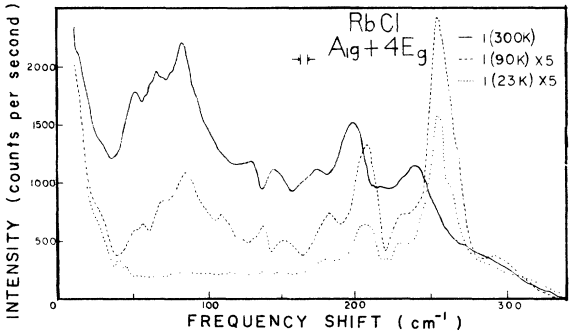

FIG. 10. Temperature dependence of the second-order Raman spectrum of RbCl; $A_{1g}+4E_g$ symmetry.

the lower frequencies, the observed $I(300):I(90)$ ratios agree with the calculated values much better than the $I(90):I(23)$ ratio. This is because the estimate of $I(23)$ is poor as the low-frequency bands ride on the background of the Rayleigh line.

The neutron measurements of Raunio and Rolandson[22] have shown that the LA(X) and LO(Γ) frequencies decrease in going from 300 to 80 K by 0.4 and 3 cm^{-1}, respectively. This could be visible in a combination such as LO – TO(Γ) which would shift from 58 to 49 cm^{-1} in going from 300 to 80 K. Such a change was not noticeable because no combination with LO(Γ) is predominant in the spectrum. The shifts in the other bands are close to the values expected from the neutron data.

E. RbBr

Figures 13–15 show the Raman spectra of RbBr. The Raman spectra of RbBr have not been published before. Appendix A gives our peak assignments based on the neutron data of Rolandson and Raunio.[23] The intensity ratios at 300 K for $I(A_{1g}):I(T_{2g}):I(E_g)$ is 50 : 5 : 1.

The temperature dependence is also observed in the figures. The intensity ratios for the main peaks are given in Table VII. The agreement between observed and calculated values is good. The frequency shifts are consistent with the values expected from the neutron data. Although the neutron data do not extend as low as 23 K, these Raman scattering data indicate that the frequency shift from 90 to 23 K is extremely small, of the order of 2% at most.

F. RbI

Figures 16–18 show the Raman spectra of RbI. The Raman spectrum RbI at room temperature has been studied by Krauzman[1] and Krishnamurty.[5] The neutron data were not available at the time. Appendix A shows our assignments based on the neutron data of Raunio and Rolandson.[24] The ratio $I(A_{1g}):I(T_{2g}):I(E_g)$ is 10 : 2 : 1.

The comparison between calculated and theoretical values of the intensity ratio for the most intense peaks is shown in Table VIII. The agreement is fairly good for the higher-frequency peaks, with the discrepancy between calculated and theoretical values for the lower-frequency region being greater. Again, the frequency shifts between 300 and 90 K are consistent with those observed in Ref. 24.

V. DISCUSSION

The Raman scattering spectra of pure KCl, KBr,

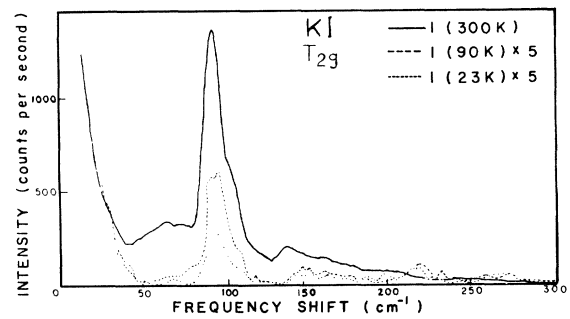

FIG. 9. Temperature dependence of the second-order Raman spectrum of KI; T_{2g} symmetry.

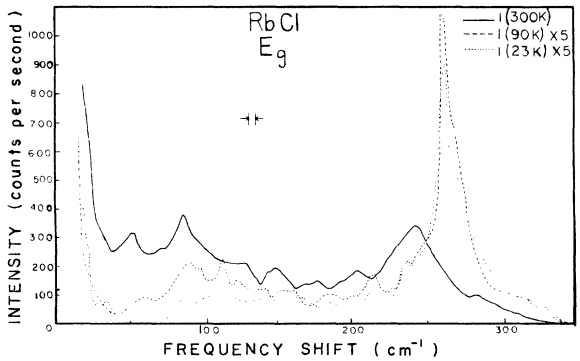

FIG. 11. Temperature dependence of the second-order Raman spectra of RbCl; E_g symmetry.

TABLE V. Temperature dependence of some features of KI second-order Raman spectrum.

Raman shift (cm^{-1}) (300 K)	Combinations contributing to the band	Intensity ratio $I(300):I(90):I(23)$ Calculated	Observed
65	TO − LA(X)	220: 24: 1	68: 8: 1 (combined)
91	2TA(Σ')	21: 3: 1	20: 3: 1 (combined)
92	TA + LA(Δ)	25 : 3.6 : 1	25 : 2.5 : 1 (combined)
101	2LA(X)	20 : 3 : 1	20 : 2 : 1 (combined)
104	TA + LA(Σ)		
185	LO + LA(Σ)	16 : 3.5 : 1	8 : 1.2 : 1 (combined)

KI, RbCl, RbBr, and RbI and their temperature dependences have been studied in the present work. Certain general features of the scattering emerge from the study.

With the aid of dispersion curves of the crystal and the selection rules, it is possible to account for almost all of the observed features as being due to second-order scattering from phonon combinations near critical points. The reason that a linear combination is adequate, instead of a rigorous convolution of one-phonon densities, to yield the two-phonon density is the small magnitude of the photon wave vector in comparison to the Brillouin zone. There are, however, a few features that cannot be identified by a critical point analysis. This indicates that detailed lattice-dynamical calculations of the Raman spectra are necessary for complete identification of the bands, a point noted by many workers for some time.

In most critical point analyses, it has been customary to confine oneself primarily to the zone-boundary points. This work indicates that at least some of the interior points, known to be major critical points in the fcc alkali halides, should be included in the analysis for a complete indexing.

Though a one-phonon density-of-states peak for a given phonon indicates that this phonon is one of the primary contributors in the combination scattering, the strength of the peak is not indicative of the relative importance of the corresponding Raman peaks. Thus, while the density of states is one of the factors determining the peak frequency, it is clear that more information is required to predict the peak intensities.

The decrease in the density of states soon after the predominant one-phonon peak at TO or LO(X) is reflected in all the second-order Raman spectra by the corresponding decrease at twice this frequency.

As an inspection of Figs. 1–18 indicates, the A_{1g} component of the scattered intensity is always strongest, followed by T_{2g} and E_g which are usually an order of magnitude weaker. This must partly be due to the fact that most combinations contain an A_{1g} component in the reduction. The total Raman-scattered intensity decreases in the order RbI: KI: RbBr: KBr: RbCl: KCl. This is in the decreasing order of the magnitude of the polarizability.[25] This simple correspondence with the magnitude of the polarizability is of interest as the Raman-scattered intensity should depend on the second-order polarizability derivatives rather than on the polarizability itself.

It would be of interest to attempt a comparison of spectra for different crystals to see whether there are regularities, similarities, or systematic trends. Such an analysis has been done by Bilz *et al.*[26] for the two-phonon infrared absorption data for silicon, germanium, and diamond. In

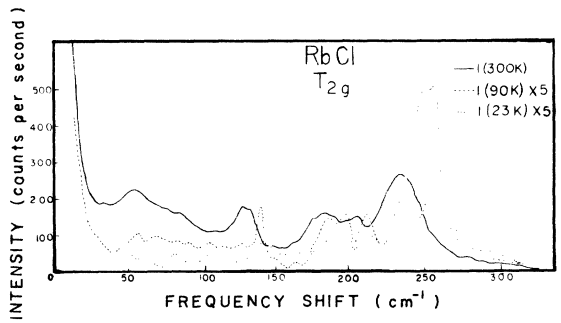

FIG. 12. Temperature dependence of the second-order Raman spectrum of RbCl; T_{2g} symmetry.

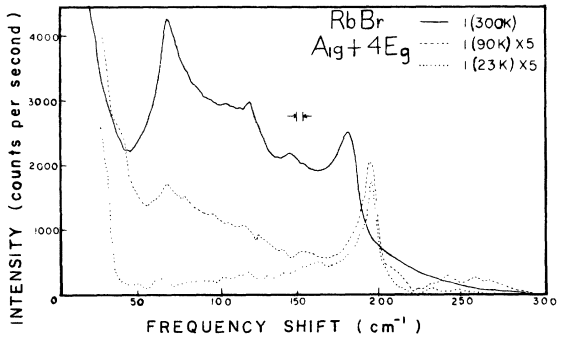

FIG. 13. Temperature dependence of the second-order Raman spectrum of RbBr; $A_{1g}+4E_g$ symmetry.

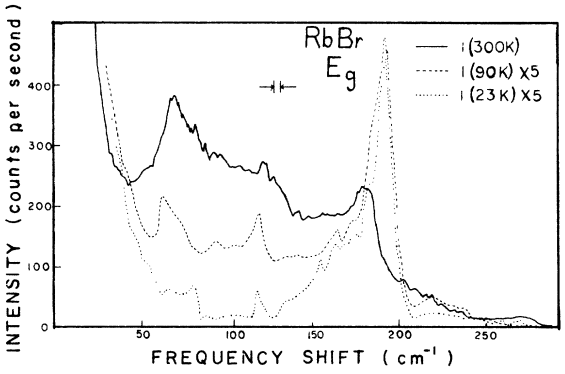

FIG. 14. Temperature dependence of the second-order Raman spectrum of RbBr; E_g symmetry.

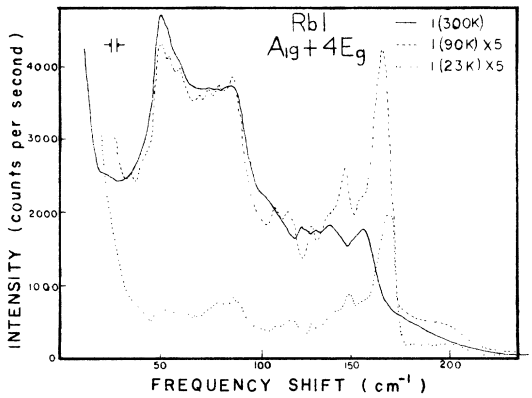

FIG. 16. Temperature dependence of the second-order Raman spectrum of RbI; $A_{1g}+4E_g$ symmetry.

that case, when the absorption was plotted as a function of reduced frequency (frequency divided by the one-phonon Raman frequency), it was seen that many features in the spectrum of silicon were also found in the spectrum of germanium, and in both cases arose from the same two-phonon combinations. However, diamond was seen not to be homologous.

Alkali halides do not have a one-phonon Raman frequency, and have two different atoms per unit cell. The appropriate scaling parameter would then probably be the maximum lattice frequency because this contains both the force constants and reduced mass of the unit cell. For example, the maximum lattice frequencies for KBr and KI are 164 and 141 cm^{-1}, respectively. In the T_{2g} spectrum for KBr (Fig. 6) a strong peak is seen at 121 cm^{-1} at 300 K. This peak is the strongest feature in the T_{2g} spectrum. One might then ask whether a comparable feature is found at 121/164 $= x/141$, or at 104 cm^{-1} in KI. Indeed, in the T_{2g} spectrum for KI (Fig. 9) one can see a shoulder at about 104 cm^{-1}. However, this is a shoulder on the high-frequency side of the main T_{2g} peak at 92 cm^{-1}. In short, the main feature in KBr does not scale over to the same feature in KI if one uses the maximum lattice frequencies for the scaling parameter.

The situation is even worse if one looks at the T_{2g} spectra for our other four systems. A single strong peak dominates the T_{2g} spectrum only in the case of RbI (Fig. 18). For KCl (Fig. 3), RbCl (Fig. 12), and RbBr (Fig. 15) the maximum intensity occurs at the high end of the frequency range. Further, in the 23 K spectra, where the greatest detail can be seen, one notes that the number of features in a spectrum (peaks, shoulders, etc.) is not the same for all hosts. In RbI we see 19 distinguishable features while in RbBr there are 23. Thus, while a feature in one crystal's spectrum may scale over to a feature (perhaps of a different kind) in another crystal's spectrum, there does not seem to be any way to adjust the frequency shift scales to bring the different spectra into registry. Our six hosts do not seem to have homologous T_{2g} spectra; no two hosts seem to have homologous spectra.

Examination of the figures shows that comparable conclusions must be drawn for the E_g and A_{1g} spectra as well. This conclusion suggests that an adequate explanation for second-order Raman

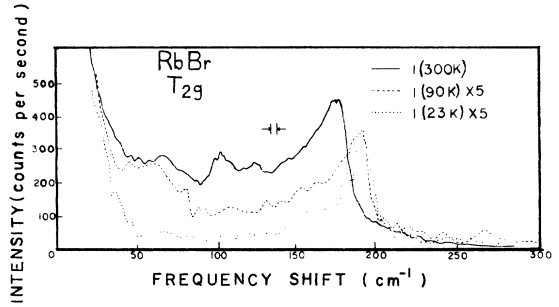

FIG. 15. Temperature dependence of the second-order Raman spectrum of RbBr; T_{2g} symmetry.

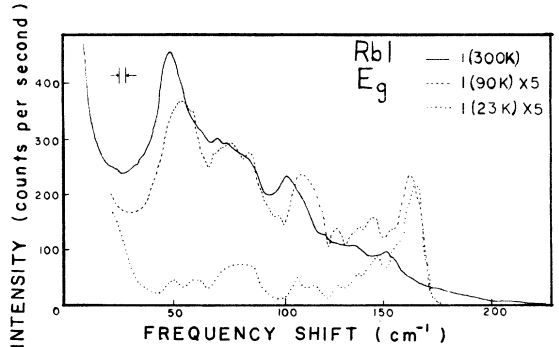

FIG. 17. Temperature dependence of the second-order Raman spectrum of RbI; E_g symmetry.

TABLE VI. Temperature dependence of some features of RbCl second-order Raman spectrum.

Raman shift (cm^{-1}) (300 K)	Combinations contributing to the band	Intensity ratio $I(300):I(90):I(23)$ Calculated	Observed
51	LO − LA(Σ)	3300: 300: 1	27.5: 2.5: 1 (combined)
85	2TA(X)	22.5: 3.5: 1	21: 3: 1 (combined)
	TO − TA(Δ)	39: 5: 1	
128	2TA(L)	12: 2.5: 1	10: 2: 1 (combined)
205	LO + LA(X)	7: 1.5: 1	12: 2: 1 (combined)
232	2TO(Δ)	5: 1.5: 1	4: 1.5: 1 (combined)

spectra rests in the details of the lattice dynamics, and emphasizes yet again the necessity for further calculations of the sort done in Ref. 11.

The different temperature dependences for difference and summation bands are clearly illustrated in the results. The predominant temperature dependence is the phonon occupation number which occurs in the final-state density-of-states factor in the scattering cross section. Anharmonic effects (frequency shifts and narrowing of lines) are also apparent.

APPENDIX A

In this Appendix we discuss the assignments of features in our data using critical point analyses for all six systems studied here. These may be useful to the reader who wishes to make a more detailed analysis of our data. Critical point analyses were published previously for KCl,[1] KBr,[17] and KI.[1] However, inelastic neutron data were not available for KCl at the time Krauzman published his results, so he made his assignments by comparing his KCl data with the spectrum for NaCl. We have used the dispersion curves obtained by Copley, MacPherson, and Timusk[19] to prepare a corrected analysis for KCl. Analyses have not been published before for RbCl, RbBr, and RbI. We have used the dispersion curves obtained by Raunio and Rolandson[22] for RbCl, Rolandson and Raunio[23] for RbBr, and Raunio and Rolandson[24] for RbI to prepare critical point analyses for these three systems. Because the previous analysis for KBr[1,17] agrees so well with ours we do not repeat a critical point analysis here, but instead point out the slight differences seen in our work.

KCl

Assignments for the main second-order features are given in Table IX. An examination of the table shows that the combinations at X account for more than half the number of features. Other frequently occurring points in the assignment are W and the point denoted by Σ in the table.

Copley *et al.*[19] point out that the strongest peak at 155 cm^{-1} (at 115 K) in the KCl one-phonon density of states arises from a saddle point in the sixth branch rather than from any of the symmetry points. It therefore seems that this point should be taken into consideration in accounting for the combinations. The TO(X) and the LO(L) frequencies are, however, at 151 and 153 cm^{-1}, respectively, very close to the saddle-point frequency. Thus, it is not possible to decide whether the intense bands in the region 300–305 cm^{-1} are due to combinations involving the saddle point rather than or in addition to those with TO(X) and LO(L) frequencies.

A secondary density-of-states peak corresponds to 107 cm^{-1}(115 K) and arises from a degeneracy of a maximum at L and a saddle point at the point (0.51, 0.51, 0) (i.e., a point on Σ with a value of $q = 0.51\pi/a$ where a is the cubic lattice parameter.) This saddle point on Σ appears important as it is one of the points whose frequencies must be used to account for a number of the features in the spec-

TABLE VII. Temperature dependence of some features of RbBr second-order Raman spectrum.

Raman shift (cm^{-1}) (300 K)	Combinations contributing to the band	Intensity ratio $I(300):I(90):I(23)$ Calculated	Observed
68	LO − TA(X)	104: 10: 1	90: 8: 1
69	2TA(X)	34: 3.4: 1	32: 4: 1
100	$2TA_1(W)$	20: 3: 1	30: 3: 1
177	2TO(Γ)	8: 1.5: 1	7: 1.1: 1
180	2LO(W)	7.2: 1.5: 1	7: 1.5: 1

TABLE VIII. Temperature dependence of some features of RbI second-order Raman spectrum.

Raman shift (cm^{-1}) (300 K)	Combinations contributing to the band	Intensity ratio $I(300):I(90):I(23)$ Calculated	Observed
51	$2TA(X)$	45: 5: 1	19: 4: 1 (combined)
75	$TA+LA(X)$	38: 5: 1	27: 3: 1 (combined)
88	$2LA(X)$	15: 3: 1	16: 2.2: 1 (combined)
113	$TO_1+TA_1(\Sigma)$	8: 2.5: 1	7.5: 2: 1 (combined)
157	$2LO(X)$	3: 1.4: 1	3: 1.3: 1 (combined)

trum. This is the only interior point in the Σ direction that is used, and hence the symbol Σ in the table stands specifically for this point. Another point that is used in the assignment is the point W; both the W_3 and W_1 branches have turning points in the dispersion curve.

The apparent cutoff of the spectrum occurs around 315–320 cm^{-1}, far below the value of twice the frequency of the LO(Γ) phonon (426 cm^{-1}) which is the theoretical cutoff of the spectrum. The reason for this probably lies in the fact that the one-phonon density of states falls rather sharply (to 3% of its peak value at 155 cm^{-1}) at 160 cm^{-1}.

KBr

Our results agree well with those published by others.[1,17] The only significant difference is a shoulder on the peak centered at 217 cm^{-1}, seen here. This appears to be a $TO+LA(X)$ peak, predicted by Burstein *et al.*,[17] but not previously observed. Unlike KCl, the cutoff for the KBr spectrum occurs close to 330 cm^{-1}, which is nearly twice the LO(Γ) frequency (332 cm^{-1}).

TABLE IX. Assignments of Raman features in KCl.

Raman frequency (cm^{-1}) at 300 K	90 K	23 K	Observed symmetry	Possible two-phonon combinations at critical points	Calculated frequency (cm^{-1}) (neutrons, 115 K)
50	45	45	T	$LO-TA\{z\}(\Sigma)$	48
				$LA-TA(X)$	48
50	52	55	A, E	$LO-LA(X)$	50
58	58	58	A, E, T		
62	62	62	T		
64	67	68	A, E	$LO-TO(\Gamma)$	67
65	68	68	T	$LO-LA(W)$	68
				$TO\{xy\}-TA\{xy\}(\Sigma)$	69
78	78	78	T		
83	94		A, E		
88	90	95	T	$TO\{z\}-TA\{xy\}(\Sigma)$	85
90	92	105	A, E	$LO-TA\{xy\}(\Sigma)$	91
95	105		A, E	$LO-TA(X)$	98
118	118	118	A, E, T	$2TA(X)$	118
	165		T	$LA+TA(X)$	166
175	185	190	A, E, T	$2TA(L)$	176
				$LO+TA(X)$	216
217	220	225	A, E, T	$2LA(X)$	214
				$2TA\{xy\}(\Sigma)$	220
				$LO+LA(W)$	230
242	250	252	A, E, T	$2TO(L)$	248
255	258	258	A, E	$LO+LA(X)$	264
	270	278	E	$LO+TO(L)$	276
282	302	302	T	$LO+TO(W)$	282
*290	312	315	A, E	$2TO(\Gamma)$	292
*290	307	309	T	$2LO; 2LA; LA+LO(L)$	306
				$LO+TO(X)$	308
				$2TO(X)$	302
				$2TO\{xy\}(\Sigma)$	304

TABLE X. Assignments of Raman features in KI.

Raman frequency (cm^{-1}) 300 K	90 K	23 K	Observed symmetry	Possible two-phonon combinations at critical points	Calculated frequency (95 K)
	45		E	TO − LA(Δ)	44
51	51	51	A, E	2TA(Δ)	50
65	65	66	T	TO − LA(X)	57
*65	65	65	E	2TA(X)	62
				LO − LA(X)	60
63	68	68	A	TO − TA(Σ)	66
70	70	70	E		
	77			2TA(Σ)	80
80	80	80	E, T	LO − TA(X)	81
				LA + TA(X)	84
				TO − TA(Δ)	85
*91		95	A, E	2TA(Σ′)	92
*92	95	95	T	TA + LA(Δ)	91
101	101	102	A, E	2LA(X)	104
104	105	105	A, E, T	LA + TA(Σ)	106
108	108	108	T	2TA(L)	110
118		118	E	LA + TA(L)	124
140	140	144	E	TO + TA(X)	140
140	140	146	T	LO + TA(X)	143
145	150	152	A	TO + TA(Σ)	146
	150		T	LO + TA(Δ)	150
				TO + TA(Σ′)	156
154	154	154	E	TA + LO(Σ′)	156
167		169	A, E, T	LO + LA(X)	164
				TO + LA(Σ)	172
163	170	171	A, E		
185		187	A, E, T	LO + LA(Σ)	182
219			T		
219		221	E	TO + LO(X)	229
228		230	E	TO + LO(Δ)	235
256		268	E	2LO(L)	262
271			E		
284			A, E	2LO(Γ)	284

KI

Our data at 300 K and assignments, based on the neutron data of Dolling *et al.*,[27] agree with those obtained by Krauzman.[1] Our data for the E_g polarization, however, show many more features than Krauzman's. Table X indicates again that combinations at X point are the most important in accounting for second-order scattering. Combinations at the Σ point (as defined in the discussion for KCl) and at L are also observed. However, two other interior points are necessary to account for the KI data. These are indicated by Δ and Σ′ in the table and are the points (0.5, 0, 0) on Δ and (0.8, 0.8, 0) on Σ [with the point X defined as (1, 0, 0)]. The point Σ′ is the point at which the longitudinal and transverse branches cross both in the acoustic and optic region. Both the frequency values at Σ′ also correspond to maxima in the one-phonon density of states. (Alternate assignments for these features may be combinations at W, but Ref. 27 does not give the dispersion curve at W.) The strongest peaks in the density of states correspond to TO(X), TO(L), TA(L), LA(X), LA(Δ), LA(Σ′), LO(X), LO(Σ), and LO(Σ′) frequencies in order. One of the strongest E_g peaks appears to correspond to 2TA(Σ′) and was not identified (observed) in Krauzman's work. The 2TA(Σ′) combination should also have a T component which must overlap with the TA + LA(Δ) peak.

The KI spectrum is the most intense of the potassium halides, as might have been expected from the high polarizability.[25] The A_{1g} and E_g spectra are most intense in the difference band region, more than half the total intensity of scattering being concentrated there. The T_{2g} spectrum has almost all the intensity concentrated in a single asymmetric band, centered at 92 cm^{-1} (300 K) consisting predominantly of the TA + LA(Δ) scattering. The apparent asymmetry is probably due to the overlap of the T components of the LA + TA(Σ) and 2TA(L) combinations.

RbCl

The Raman spectrum of RbCl has been studied by Stekhanov and Korol'kov.[6] However, the data were taken with unpolarized light and no assignments of the features as phonon combinations were made. Our assignments are given in Table XI.

Again all the predominant features can be accounted for as arising from phonon combinations at X, L, Δ, and Σ, the two latter points being defined as before. These points are also the major critical points of RbCl. The A_{1g} component of the scattered intensity is concentrated mostly in the difference-band region while the E_g and T_{2g} is concentrated in the summation bands. RbCl has a gap in the phonon distribution from 99 to 109 cm^{-1} at 80 K, disappearing at 300 K. There is no indication of this in the spectra. The spectrum has an apparent cutoff at 290 cm^{-1} whereas the 2LO(Γ) value is 350 cm^{-1}. The features at 357, 364, and 432 cm^{-1} observed by Stekhanov and Korol'kov were not observed by us.

RbBr

Our assignments are given in Table XII where

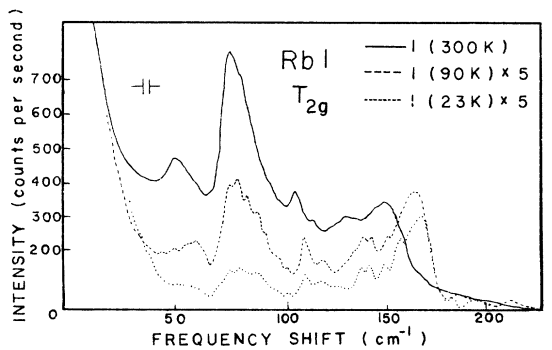

FIG. 18. Temperature dependence of the second-order Raman spectrum of RbI; T_{2g} symmetry.

TABLE XI. Assignments of Raman features in RbCl.

Raman frequency (cm^{-1}) at 300 K	90 K	23 K	Observed symmetry	Possible two-phonon combinations at critical points	Calculated frequency (80 K)
51	55	55	A, E	LO − LA(Σ)	46
55	58	62	T	$TO_2 - TA_1(\Sigma)$	58
66	66		A, E	2TA(Δ)	67
*85	87	87	A, E	2TA(X)	88
				TO − TA(Δ)	89
	105	108	T	LO − TA(Δ)	105
128	140	145	T	2TA(L)	138
130	137	138	A, E	TO + TA(Δ)	141
147	150	152	A, E	2LA(X)	152
174	184	184	A, E	2LA(Σ)	180
				$TO_1 + TA_1(\Sigma)$	186
177	187		T	2LA(Δ)	184
185	198		T	TA_1 + LO(Σ)	194
200	210	212	A	2LA(L)	202
205	215	215	E	TO_2 + LA(Σ)	206
208			T	LO + LA(X)	210
				TO + LA(X)	203
220	230	230	A	LO + LA(Δ)	231
	235	235	E	2TO(Σ)	232
*232	250	253	T	2TO(Δ)	254
*245	260	260	A, E	$LO + TO_1(\Sigma)$	264
	257	258	T	LO + TO(X)	261
	265	267	T	LO + TO(Δ)	266
290			A	2LO(L)	296

TABLE XII. Assignments of Raman features in RbBr.

Raman frequency (cm^{-1}) at 300 K	90 K	23 K	Observed symmetry	Possible two-phonon combinations at critical points	Calculated frequency (80 K)
27	31		T	LA − TA(X)	26
				TO − LA(X)	34
				$TO_2 - TA_1(\Sigma)$	32
	37	37	T	LO − TO(Γ)	36
45	45	45	T	$TO_1 - TA_1(W)$	48
*68	72	70	T	LO − TA(X)	66
*69			E	2TA(X)	66
77	79		T		
*100	108	112	A, T	$2TA_1(W)$	98
125			E	2LA(X)	118
				TO + TA(X)	128
126	131	131	T	LO + TA(X)	132
				$LA + TA_1(\Sigma)$	132
145	155	160	A, E	$2TO_2(\Sigma)$	156
145	150	150	T	TO + LA(X)	154
145				LO + LA(X)	158
	154		E		
	165	165	E		
	175	175	E	2LA(Σ)	172
				2LA(L)	184
178	190	190	E	$2TO_1$	193
*180	195	197	A	2LO; 2TO(W)	193
*177	190	195	T	2TO(Γ)	188
				$2TO_1(\Sigma)$	198
200	220	225	E	LO + TO(Γ)	224
270			T	2LO(Γ)	260

TABLE XIII. Assignments of Raman features in RbI.

Raman frequency (cm^{-1}) at 300 K	90 K	23 K	Observed symmetry	Possible two-phonon combinations at critical points	Calculated frequency (80 K)
*51	51	51	*A*, *E*, *T*	2TA(*X*)	50
	55	55	*A*		
	60	60	*A*, *E*	TO − TA(*X*)	57
	69		*A*		
70	77	77	*A*, *E*	$2TA_1(\Sigma)$	70
*75	75	75	*A*, *T*	LA + TA(*X*)	69
				$2TA_1(\Sigma)$	70
	78	78	*T*		
	*80	80	*A*, *E*	2LA(*X*)	88
	85	85	*E*		
	102	102	*E*	$TA_1 + TO_2(\Sigma)$	103
100	107	107	*A*, *E*	2TA(*L*)	106
103	108	108	*T*	TA + TO(*X*)	107
				TA + LO(*X*)	110
	115	116	*A*, *E*	$LO + TA_1(\Sigma)$	116
113	118	118	*T*	$TO_1 + TA_1(\Sigma)$	118
123	127	127	*A*, *E*	LA + LO(*X*)	129
				2TO(*L*)	130
126	137	137	*T*	$2TO_2(\Sigma)$	136
	142	142	*T*		
140	145	145	*A*, *E*	$LO + TO_2(\Sigma)$	149
	150	158	*E*		
150	162	165	*T*	2LO(Σ)	162
151	163	165	*E*	$LO + TO_1(\Sigma)$	164
157	165	169	*A*, *E*	$2TO_1(\Sigma)$	166
				2LO(*X*)	170

it can be seen that, as before, combinations at *X* predominate in accounting for the scattering. Other frequently occurring combinations are those at Γ, *W*, and Σ, with just one combination at *L*, viz., 2LA(*L*). The main peaks in the one-phonon density of states are at LO(*X*), TO(Γ), LO(*L*), TA(*L*), TA(Σ), and TO(Σ). *W* does not appear to be one of the main critical points in the one-phonon density. All the combinations at Γ, it is observed, involve TO(Γ) which is one of the peak frequencies in the one-phonon density of states.

The A_{1g} and E_g spectra have most of the intensity in the low-frequency region at 300 K. At the lower temperatures, most of the intensity is in the band around 190 cm^{-1}. The T_{2g} spectrum is intense in the high-frequency region at 300, 90, and 23 K.

RbI

Our assignments are given in Table XIII. The RbI spectrum resembles the KI spectrum except that the frequency range is smaller for RbI. However, a detailed indexing shows that the peaks cannot be indexed by direct correspondence, as most of the combinations in the case of RbI arise from phonons at the Σ point rather than at *X* as in KI. The strong band that accounts for almost all the scattering in the T_{2g} component cannot be indexed as TA + LA(Δ) as in the case of KI but has to be assigned to TA + LA(*X*) scattering. It is not necessary to invoke combinations at the Δ point to account for any of the features in RbI. The one-phonon density peaks are close to LO(*X*), TO(*X*), LA(*X*), LA(Σ), and TO(Γ), respectively. The intensity falls off abruptly after twice the LO(*X*) frequency. This is particularly noticeable in the E_g spectrum. The intensity is predominantly in the low-frequency region.

*Work supported in part by the National Science Foundation.
†Present address: Canevin High School, Pittsburgh, Pa. 15205.
[1]M. Krauzman, C. R. Acad. Sci. **265B**, 689 (1967); C. R. Acad. Sci. **265B**, 1029 (1967); also, in *Light Scattering Spectra of Solids*, edited by G. B. Wright (Springer-Verlag, New York, 1969), p. 109.
[2]A. C. Menezies and J. Skinner, J. Phys. Radium **9**, 93 (1948).
[3]C. V. Raman, Proc. Indian Acad. Sci. A **57**, 1 (1963).
[4]R. S. Krishnan and P. S. Narayanan, Proc. Indian Acad. Sci. A **28**, 296 (1948).
[5]N. Krishnamurty, Proc. Phys. Soc. Lond. **85**, 1025 (1965).
[6]A. I. Stekhanov and A. P. Korol'kov, Fiz. Tverd. Tela **8**, 920 (1966) [Sov. Phys.-Solid State **8**, 734 (1966)].
[7]R. S. Krishnan, in *Lattice Dynamics*, edited by R. F. Wallis

(Pergamon, New York, 1965).
[8]A. A. Maradudin and S. Ushioda, J. Phys. Chem. Solids **31,** 1075 (1970).
[9]A. M. Karo and J. R. Hardy, Phys. Rev. **141,** 696 (1966).
[10]A. M. Karo, J. R. Hardy, and I. W. Morrison, J. Phys. (Paris) **26,** 668 (1965).
[11]R. A. Cowley, Proc. Phys. Soc. Lond. **84,** 281 (1964); A. D. Bruce and R. A. Cowley, J. Phys. C **5,** 595 (1972); S. L. Cunningham, J. R. Hardy and M. Hass, in *Light Scattering in Solids*, edited by M. Balkanski (Flammarion, Paris, 1971), p.257.
[12]G. P. Montgomery, Ph.D. dissertation (University of Illinois, 1971)(unpublished).
[13]I. Nair and C. T. Walker, Phys. Rev. B **3,** 3446 (1971).
[14]M. Born and K. Huang, *Dynamical Theory of Crystal Lattices* (Oxford U.P., Oxford, England, 1956).
[15]R. Loudon, Adv. Phys. **13,** 423 (1964).
[16]J. L. Birman, Phys. Rev. **131,** 1489 (1963).
[17]E. Burstein, F. A. Johnson, and R. Loudon, Phys. Rev. **139,** 1239 (1965).
[18]J. C. Phillips, Phys. Rev. **113,** 149 (1959).
[19]J. R. D. Copley, R. W. MacPherson, and T. Timusk, Phys. Rev. **182,** 965 (1969).
[20]T. Damen, S. Porto, and B. Tell, Phys. Rev. **142,** 570 (1970).
[21]A. D. B. Woods, B. N. Brockhouse, R. A. Cowley, and W. Cochran, Phys. Rev. **131,** 1052 (1963).
[22]G. Raunio and S. Rolandson, J. Phys. C **3,** 1013 (1970).
[23]S. Rolandson and G. Raunio, J. Phys. C **4,** 958 (1971).
[24]G. Raunio and S. Rolandson, Phys. Status Solidi **40,** 749 (1970).
[25]J. R. Tessman, A. H. Kahn, and W. Shockley, Phys. Rev. **92,** 890 (1953).
[26]H. Bilz, R. Geick, and K. F. Renk, in *Lattice Dynamics,* edited by R. F. Wallis (Pergamon, Oxford, England, 1965), p. 355.
[27]G. Dolling, R. A. Cowley, C. Schittenhelm, and I. M. Thorson, Phys. Rev. **147,** 577 (1966).